Dalton Transactions

PAPER

View Article Online
View Journal | View Issue

Cite this: *Dalton Trans.*, 2018, **47**, 3298

Three Zn(II)-based MOFs for luminescence sensing of Fe^{3+} and $Cr_2O_7^{2-}$ ions†

Zhi-Zun Xiao, Li-Juan Han, Zhong-Jie Wang and He-Gen Zheng *

Received 9th December 2017,
Accepted 22nd January 2018

DOI: 10.1039/c7dt04659f

rsc.li/dalton

Three zinc metal–organic frameworks (MOFs), $\{ZnL(chd)\}_n$ (**1**), $\{[Zn(L)_{0.5}(oba)]\cdot DMF\cdot H_2O\}_n$ (**2**) and $\{[Zn(L)_{0.5}(sdb)]\cdot H_2O\}_n$ (**3**) [L = *E*,*E*-2,5-dihexyloxy-1,4-bis-(2-pyridin-vinyl)-benzene; H_2chd = 1,4-cyclohexanedicarboxylic acid, H_2oba = 4,4′-oxybisbenzoic acid, H_2sdb = 4,4′-sulfonyldibenzoic acid], have been hydrothermally synthesized. We explored their applications in detecting ions, and the result shows that they all show highly selective sensing for Fe^{3+} and $Cr_2O_7^{2-}$ ions.

Introduction

In recent years, metal–organic frameworks (MOFs) have attracted considerable attention because of their fascinating structures and properties. They have significant potential value in gas storage and separation,[1–3] luminescence,[4–6] and catalysis.[7–10] As is known, Fe^{3+} is a kind of ample trivalent metal ion for all organisms and plays a vital role in various crucial processes. Both iron shortage and excess will result in various serious conditions and disorders, such as skin diseases, iron deficiency anemia (IDA), agrypnia, and decreased immunity. Though Fe^{3+} is very important for organisms, it can also cause environmental contaminantion.[11] Meanwhile, $Cr_2O_7^{2-}$ with high toxicity and carcinogenicity has been used in industrial processes. Thus, detecting them in the environment effectively has been a hot topic for chemists.

At present, there are many kinds of methods to detect these contaminants, the applications of which are, however, greatly limited due to shortcomings, such as low portability, complex pretreatments, and expensive instruments. Fortunately, recent studies show that the fluorimetric method based on luminescent metal–organic frameworks (MOFs) as probes has unique advantages, such as nondestructive detection, high sensitivity, fast response time, and real-time monitoring.[12–16]

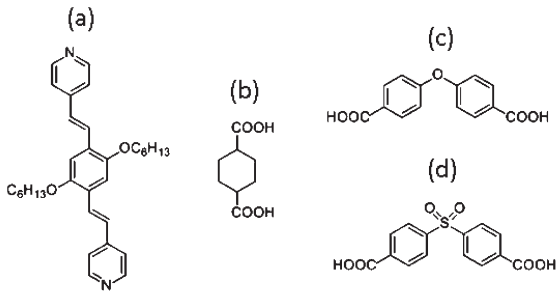

Scheme 1 (a) *E*,*E*-2,5-Dihexyloxy-1,4-bis-(2-pyridin-vinyl)-benzene (L); (b) 1,4-cyclohexanedicarboxylic acid (H_2chd); (c) 4,4′-oxybisbenzoic acid (H_2oba); (d) 4,4′-sulfonyldibenzoic acid (H_2sdb).

In this work, we report three new zinc compounds, $\{ZnL(chd)\}_n$ (**1**), $\{[Zn(L)_{0.5}(oba)]\cdot DMF\cdot H_2O\}_n$ (**2**) and $\{[Zn(L)_{0.5}(sdb)]\cdot H_2O\}_n$ (**3**) [L = *E*,*E*-2,5-dihexyloxy-1,4-bis-(2-pyridin-vinyl)-benzene; H_2chd = 1,4-cyclohexanedicarboxylic acid, H_2oba = 4,4′-oxybisbenzoic acid, H_2sdb = 4,4′-sulfonyldibenzoic acid] (Scheme 1). Compound **1** is a 2-fold interpenetrated **dia** network with the point symbol of $\{6^6\}$. Compound **2** features a **mab** self-penetrated network with the point symbol of $(4^4\cdot6^{10}\cdot8)$. And compound **3** is a 4-connected **sql** network with the point symbol of $\{4^4.6^2\}$. With respect to aqueous systems used in many reports,[17,18] we use the DMF system, and fluorescence titrations confirm that MOFs **1–3** show excellent potential in sensing Fe^{3+} and $Cr_2O_7^{2-}$ in the DMF system. Quenching mechanisms have also been studied.

Experimental section

Materials and general methods

IR spectra were recorded on a Nicolet (Impact 410) spectrometer with KBr pellets (5 mg of the sample in 300 mg of KBr)

State Key Laboratory of Coordination Chemistry, School of Chemistry and Chemical Engineering, Collaborative Innovation Center of Advanced Microstructures, Nanjing University, Nanjing 210093, P. R. China. E-mail: zhenghg@nju.edu.cn; Fax: +86-25-83314502

†Electronic supplementary information (ESI) available: Experimental procedures, tables of crystal data and geometric parameters, figures showing thermogravimetric analysis, XRD, and CIF files for **1–3**. CCDC 1589901–1589903. For ESI and crystallographic data in CIF or other electronic format see DOI: 10.1039/c7dt04659f

in the range of 400–4000 cm^{-1}. C, H and N elemental analysis was performed with a PerkinElmer 240C elemental analyzer. The as-synthesized compounds were characterized by thermogravimetric analyses (TGA) on a PerkinElmer thermogravimetric analyzer, Pyris 1 TGA, up to 650 K using a heating rate of 10 K min^{-1} under a N_2 atmosphere. Powder X-ray diffraction (PXRD) measurements were performed on a Bruker D8 Advance X-ray diffractometer by using Cu-Kα radiation (1.5418 Å), and the X-ray tube was operated at 40 kV and 40 mA.

Synthesis of *E*,*E*-2,5-dihexyloxy-1,4-bis-[2-pyridin-vinyl]-benzene (L). 1,4-Dibromo-2,5-dihexyloxybenzene (2.18 g, 5 mmol), 4-vinylpyridine (1.6 g, 15 mmol), $Pd(OAc)_2$ (36 mg, 3% mmol), tris(2,4,6-trimethoxyphenyl)phosphine (106 mg, 4% mmol), Et_3N (5 ml) and CH_3CN (35 ml) were mixed in a 100 mL Schlenk flask and refilled with N_2 three times. The reaction solution was heated at 93 °C for 3 days. The resulting mixture was concentrated *in vacuo*. The crude product was purified with column chromatography on silica gel eluted with petroleum ether/ethyl acetate (1 : 3, v/v) to give the product as a yellow solid (2.0 g, 82%). ^{1}H-NMR (400 MHz, $CDCl_3$): δ 8.58 (d, J = 6.1 Hz, 4H), 7.67 (d, J = 16.5 Hz, 2H), 7.38 (d, J = 6.1 Hz, 4H), 7.13 (s, 2H), 7.08 (d, J = 16.5 Hz, 2H), 4.08 (t, J = 6.5 Hz, 4H), 1.94–1.84 (m, 4H), 1.61–1.50 (m, 4H), 1.45–1.33 (m, 8H), 0.91 (t, J = 7.1 Hz, 6H). The IR spectroscopy of H_2L is shown in Fig. S4.†

Synthesis of {ZnL(chd)}$_n$ (1). A mixture of H_2L (4.8 mg, 0.01 mmol), H_2chd (3.3 mg, 0.02 mmol), $Zn(NO_3)_2{\cdot}6H_2O$ (31 mg, 0.1 mmol), DMF (4.0 mL) and H_2O (2.5 mL) was placed in a 20 ml glass vial and heated at 100 °C for 3 days. The resulting yellow block crystals were washed with fresh DMF, and collected. Yield: 53% (based on the H_2L ligand). Elemental analysis of **1**, calculated for $C_{40}H_{50}ZnN_2O_6$: C, 66.71%; H, 7%; N, 3.89%. Found: C, 66.72%; H, 7.05%; N, 3.81%. The IR spectroscopy of complex **1** is shown in Fig. S5.†

Synthesis of {[Zn(L)$_{0.5}$(oba)]·DMF·H$_2$O}$_n$ (2). A mixture of H_2L (4.8 mg, 0.01 mmol), H_2oba (5.1 mg, 0.02 mmol), $Zn(NO_3)_2{\cdot}6H_2O$ (31 mg, 0.1 mmol), DMF (3.5 mL) and H_2O (1.5 mL) was placed in a 20 ml glass vial and heated at 100 °C for 3 days. The resulting yellow block crystals were washed with fresh DMF, and collected. Yield: 47% (based on the H_2L ligand). Elemental analysis of **2**, calculated for $C_{33}H_{37}N_2O_8Zn$: C, 60.51%; H, 5.69%; N, 4.28%. Found: C, 60.55%; H, 5.21%; N, 4.35%. The IR spectroscopy of complex **2** is shown in Fig. S6.†

Synthesis of {[Zn(L)$_{0.5}$(sdb)]·H$_2$O}$_n$ (3). A mixture of H_2L (4.8 mg, 0.01 mmol), H_2sdb (6.1 mg, 0.02 mmol), $Zn(NO_3)_2{\cdot}6H_2O$ (31 mg, 0.1 mmol), DMF (3.0 mL) and H_2O (3.0 mL) was placed in a 20 ml glass vial and heated at 100 °C for 3 days. The resulting orange block crystals were washed with fresh DMF, and collected. Yield: 49% (based on the H_2L ligand). Elemental analysis of **3**, calculated for $C_{30}H_{30}ZnNO_8S$: C, 57.19%; H, 4.80%; N, 2.22%. Found: C, 57.13%; H, 4.81%; N, 2.25%. The IR spectroscopy of complex **3** is shown in Fig. S7.†

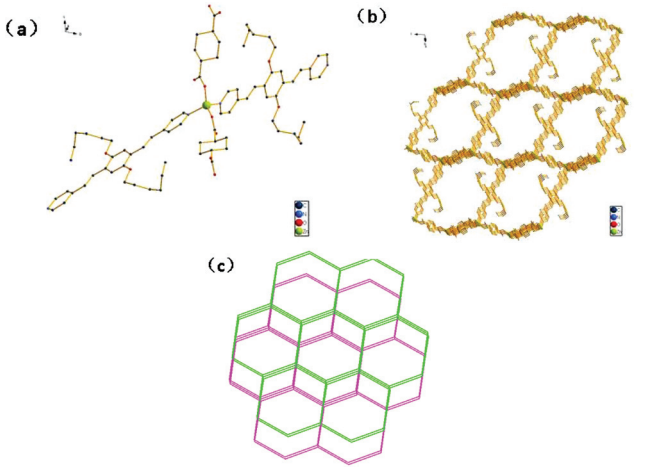

Fig. 1 (a) Coordination environment of the Zn(II) ion in **1**. (b) A single 3D network of **1**. (c) Schematic representation of a 2-fold interpenetrated **dia** network of **1**.

Results and discussion

Description of the crystal structure of {ZnL(chd)}$_n$ (1)

Single-crystal structure analysis reveals that **1** crystallizes in the triclinic crystal system with the $P\bar{1}$ space group. The asymmetric unit of **1** consists of one Zn(II) metal center, one L ligand and one chd^{2-} anion. As shown in Fig. 1a, each Zn(II) center is four-coordinated by two oxygen atoms from two different chd^{2-} anions and two nitrogen atoms from two L ligands to form a distorted tetrahedral coordination geometry. In the crystal structure of **1**, both the L ligands and chd^{2-} anions act as bridging μ_2 modes to link two metal ions. The three-dimensional framework is generated from the extension of the adjacent Zn ions by the connection of H_2chd ligands and L ligands (Fig. 1b).

To better understand the nature of this intricate framework, we apply a topological approach, which reduces multidimensional structures to simple nodes and connection nets. The Zn

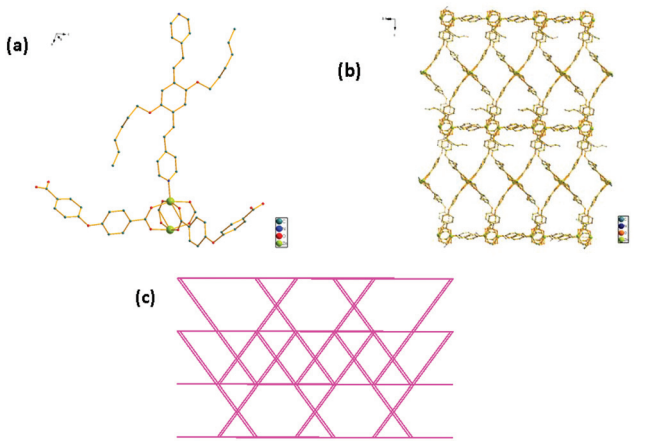

Fig. 2 (a) Coordination environment of the Zn(II) ion in **2**. (b) A single 3D network of **2**. (c) Schematic representation of a **mab** self-penetrated network of **2**.

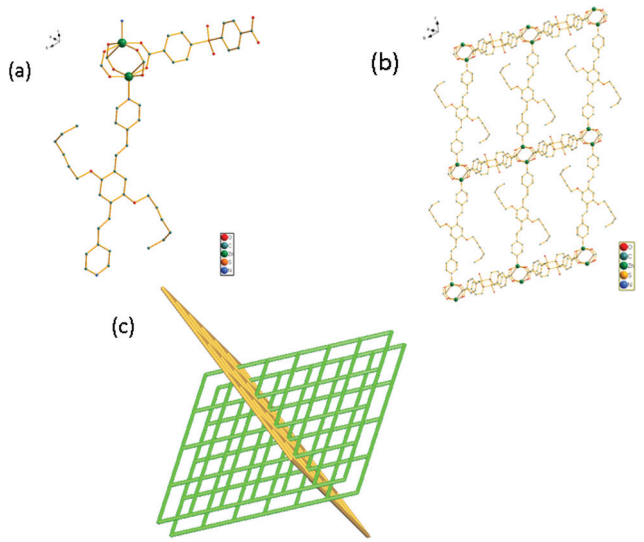

Fig. 3 (a) Coordination environment of the Zn(II) ion in **3**. (b) Views of 2D sheets. (c) Schematic representation of the **sql** polycatenation of **3**.

ions can be regarded as 4-connected nodes and the two ligands act as linkers. Thus, the whole structure can be characterized as a 2-fold interpenetrated **dia** network with the point symbol of $\{6^6\}$ (Fig. 1c).

Description of the crystal structure of $\{[Zn(L)_{0.5}(oba)]\cdot DMF\cdot H_2O\}_n$ (2)

Compound **2** crystallizes in the monoclinic crystal system with the $P2_1/c$ space group. In the asymmetric unit, there are one Zn(II) metal center, a half of an L ligand, one oba^{2-} anion, one lattice DMF molecule and one lattice water molecule. Each Zn(II) center is five-coordinated by four oxygen atoms from four different oba^{2-} anions and one nitrogen atom from one L ligand to form a square pyramid. Both the L ligand and oba^{2-} act as linkers to bridge two adjacent metal ions. Four carboxylate groups from four different oba^{2-} anions connect pairs of Zn ions to generate a $Zn_2(CO_2)_4$ dimer. The $Zn_2(CO_2)_4$ dimers are connected to four other dimers to construct grid layer motifs. And they are pillared by L ligands to establish a 3D coordination polymer network in **2** (Fig. 2b). If organic ligands are considered as linkers, $Zn_2(CO_2)_4$ dimers can be identified as six-connected nodes. Thus, the topology of the structure can be simplified as a **mab** self-penetrated network with the point symbol of $(4^4\cdot6^{10}\cdot8)$ (Fig. 2c).

Description of the crystal structure of $\{[Zn(L)_{0.5}(sdb)]\cdot H_2O\}_n$ (3)

Single-crystal structure analysis reveals that **3** crystallizes in the monoclinic crystal system with the $C2/c$ space group. The asymmetric unit of **3** consists of one Zn(II) metal center, a half of an L ligand, one sdb^{2-} anion and one lattice molecule, which was removed by the SQUEEZE routine in PLATON. Each Zn(II) center is five-coordinated by four oxygen atoms from four different sdb^{2-} ligands and one nitrogen atom from one L ligand to form a square pyramid (Fig. 3a). Four carboxylate groups from four different sdb^{2-} ligands connect pairs of Zn ions to generate a dinuclear $Zn_2(CO_2)_4$ secondary building unit (SBU). The sdb^{2-} ligands connect the $Zn_2(CO_2)_4$ SBUs to form 1D chains. These 1D chains are connected by the L ligand in the axial direction to form a 2D sheet (Fig. 3b). To better understand the nature of this intricate framework, we apply a topological approach. The $Zn_2(CO_2)_4$ SBUs can be regarded as

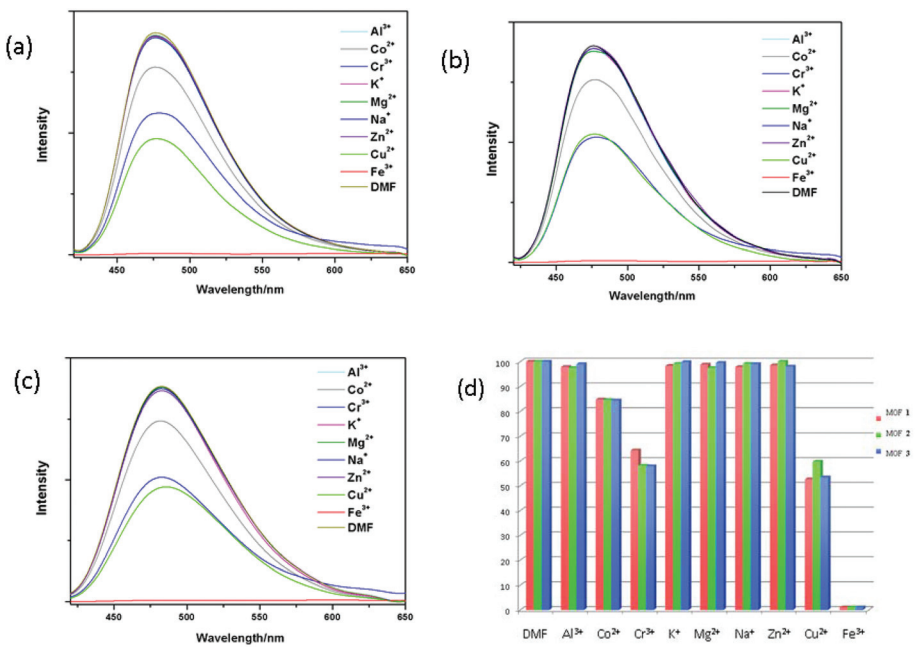

Fig. 4 (a)–(c) Fluorescence spectra of MOFs **1–3** (DMF suspension, 2.0 mL) after the addition of different metal ions (5×10^{-2} M, 50 μL). (d) The relative emission intensity in the presence of different metal ions.

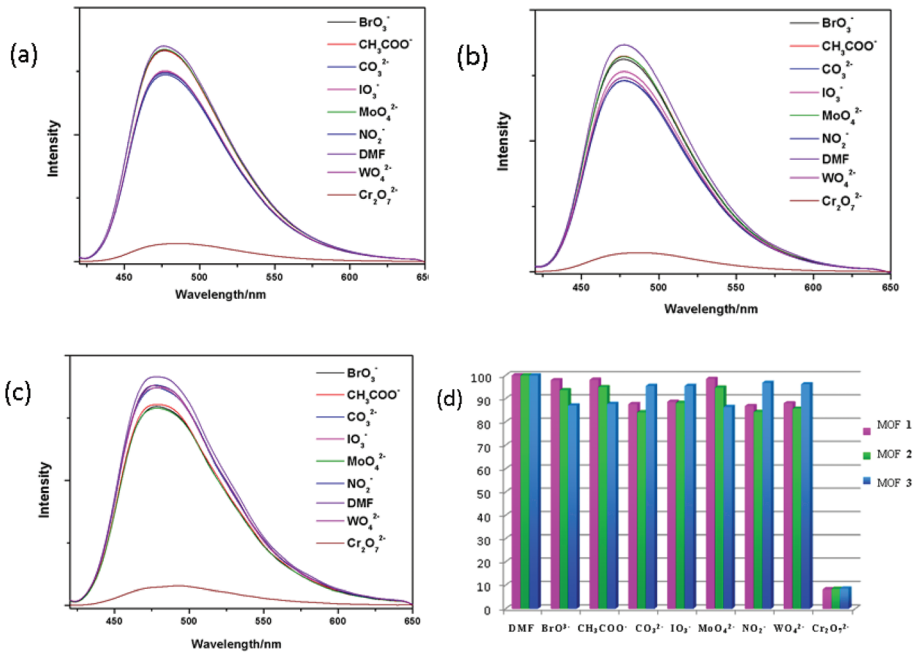

Fig. 5 (a)–(c) Fluorescence spectra of MOFs **1–3** (DMF suspension, 2.0 mL) after the addition of different anions (5×10^{-3} M, 100 μL). (d) The relative emission intensity in the presence of different anions.

4-connected nodes and the two ligands act as linkers. Thus, the whole structure can be characterized as a 4-connected **sql** network with the point symbol of $\{4^4.6^2\}$ (Fig. 3c).

Sensing of metal cations and inorganic anions

The luminescence sensing of different metal cations was performed. Different DMF solutions containing 5×10^{-2} M $A(NO_3)_X$ (A = Al^{3+}, Co^{2+}, Cr^{3+}, K^+, Mg^{2+}, Na^+, Zn^{2+}, Cu^{2+}, Fe^{3+}) were added into the suspension of MOFs **1**, **2** and **3**, respectively. As shown in Fig. 4, among the metal cations mentioned above, Fe^{3+} exhibits the most excellent quenching effect. It has the highest quenching efficiency for the three MOFs up to 99%. To elucidate the possible mechanism of luminescence quenching by Fe^{3+}, liquid UV-vis absorption spectra measurements were performed (Fig. S14†). Obviously, Fe^{3+} ions in DMF have a wide absorption band from 250 to 410 nm, which covered the range of the three MOFs. However, other ions in DMF only have an absorption band below 350 nm (Fig. S12†). Upon light excitation, there is a competition for the absorption of light source energy, and as a consequence the Fe^{3+} ions almost filtered the light adsorption; then, Fe^{3+} ions present the excellent quenching effect on these three MOFs. The quenching mechanism is consistent with other previously proposed mechanisms.[19–22]

The same procedure was carried out to investigate the luminescence sensing of different inorganic anions. Different DMF solutions containing 5×10^{-3} M Na_XM (M = BrO_3^-, CH_3COO^-, CO_3^{2-}, IO_3^-, MoO_4^{2-}, NO_2^-, WO_4^{2-}, $Cr_2O_7^{2-}$) were added into the suspension of MOFs **1**, **2** and **3**, respectively. As shown in Fig. 5, among the anions mentioned above, $Cr_2O_7^{2-}$ exhibits the most significant quenching effect. It has the highest quenching efficiency for the three MOFs up to 90%. According to the UV-vis absorption spectrum (Fig. S14†), the strong absorption bands of the $Cr_2O_7^{2-}$ solution are in the ranges of 250–420 nm, which covered the range of the three MOFs. There also exists a competition for the absorption of light source energy. As a result, $Cr_2O_7^{2-}$ ions show a good quenching effect on these MOFs. In addition, we investigated the luminescence sensing of Fe^{2+} and CrO_4^{2-}, and the results show low luminescence quenching (Fig. S11†).

Conclusions

In conclusion, three zinc metal–organic frameworks with linear pyridyl ligands have been designed and synthesized. Luminescence sensing measurements indicate that they all show highly selective sensing for Fe^{3+} and $Cr_2O_7^{2-}$ ions, which can be explained in terms of the competitive absorption of excitation wavelength energy between Fe^{3+} and $Cr_2O_7^{2-}$ ions and these three MOFs. This work indicates that zinc-based MOFs have the potential to serve as fluorescent sensors.

Conflicts of interest

There are no conflicts to declare.

Acknowledgements

This work was supported by grants from the National Natural Science Foundation of China (no. 21771101, 21371092 and 21701048).

References

1 C. X. Chen, Z. W. Wei, J. J. Jiang, S. P. Zheng, H. P. Wang, Q. F. Qiu, C. C. Cao, D. Fenske and C. Y. Su, *J. Am. Chem. Soc.*, 2017, **139**, 6034.
2 X. J. Hong, Q. Wei, Y. P. Cai, S. R. Zheng, Y. Yu, Y. Z. Fan, X. Y. Xu and L. P. Si, *ACS Appl. Mater. Interfaces*, 2017, **9**, 4701.
3 M. Witman, S. L. Ling, S. Jawahery, P. G. Boyd, M. Haranczyk, B. Slater and B. Smit, *J. Am. Chem. Soc.*, 2017, **139**, 5547.
4 X. G. Yang, X. Q. Lin, Y. B. Zhao, Y. S. Zhao and D. P. Yan, *Angew. Chem., Int. Ed.*, 2017, **56**, 7853.
5 W. Yan, C. L. Zhang, S. G. Chen, L. J. Han and H. G. Zheng, *ACS Appl. Mater. Interfaces*, 2017, **9**, 1629.
6 F. Y. Yi, Y. Wang, J. P. Li, D. Wu, Y. Q. Lan and Z. M. Sun, *Mater. Horiz.*, 2015, **2**, 245.
7 K. M. Choi, D. Kim, B. Rungtaweevoranit, C. A. Trickett, J. T. D. Barmanbek, A. S. Alshammari, P. D. Yang and O. M. Yaghi, *J. Am. Chem. Soc.*, 2017, **139**, 356.
8 Y. Z. Chen, Z. U. Wang, H. W. Wang, J. L. Lu, S. H. Yu and H. L. Jiang, *J. Am. Chem. Soc.*, 2017, **139**, 2035.
9 B. An, J. Z. Zhang, K. Cheng, P. F. Ji, C. Wang and W. B. Lin, *J. Am. Chem. Soc.*, 2017, **139**, 3834.
10 W. X. Liu, J. J. Huang, Q. Yang, S. J. Wang, X. M. Sun, W. N. Zhang, J. F. Liu and F. W. Huo, *Angew. Chem., Int. Ed.*, 2017, **56**, 5512.
11 Q. Zhao, F. Y. Li and C. H. Huang, *Chem. Soc. Rev.*, 2010, **39**, 3007–3030.
12 X. Feng, Y. Q. Feng, N. Guo, Y. L. Sun, T. Zhang, L. F. Ma and L. Y. Wang, *Inorg. Chem.*, 2017, **56**, 1713.
13 Y. Zhao, X. Y. Xu, L. Qiu, X. J. Kang, L. L. Wen and B. G. Zhang, *ACS Appl. Mater. Interfaces*, 2017, **9**, 15164.
14 T. T. Zheng, J. Zhao, Z. W. Fang, M. T. Li, C. Y. Sun, X. Li, X. L. Wang and Z. M. Su, *Dalton Trans.*, 2017, **46**, 2456.
15 S. G. Chen, Z. Z. Shi, L. Qin, H. L. Jia and H. G. Zheng, *Cryst. Growth Des.*, 2017, **17**, 67.
16 W. T. Yang, H. R. Tian, J. P. Li, Y. F. Hui, X. He, J. Y. Li, S. Dang, Z. G. Xie and Z. M. Sun, *Chem. – Eur. J.*, 2016, **22**, 15451.
17 R. Lv, H. Li, J. Su, X. Fu, B. Y. Yang, W. Gu and X. Liu, *Inorg. Chem.*, 2017, **56**, 12348.
18 T. Q. Song, J. Dong, H. L. Gao, J. Z. Cui and B. Zhao, *Dalton Trans.*, 2017, **46**, 13862.
19 F. Y. Yi, J. P. Li, D. Wu and Z. M. Sun, *Chem. – Eur. J.*, 2015, **21**, 11475.
20 J. L. Chen, F. Y. Yi, H. Yu, S. H. Jiao, G. S. Pang and Z. M. Sun, *Chem. Commun.*, 2014, **50**, 10506.
21 G. X. Wen, M. L. Han, X. Q. Wu, Y. P. Wu, W. W. Dong, J. Zhao, D. S. Li and L. F. Ma, *Dalton Trans.*, 2016, **45**, 15492.
22 H. Xu, J. K. Gao, X. F. Qian, J. P. Wang, H. J. He, Y. J. Cui, Y. Yang, Z. Y. Wang and G. D. Qian, *J. Mater. Chem. A*, 2016, **4**, 10900.